J. Fluid Mech. (1986), *vol.* 170, *pp.* 293–317
Printed in Great Britain

Spatially amplifying modes of the Charney baroclinic-instability problem

By R. T. PIERREHUMBERT
Geophysical Fluid Dynamics Laboratory/NOAA, Princeton University, NJ 08542, USA

(Received 22 August 1985 and in revised form 18 February 1986)

We determine the circumstances under which baroclinic instability in the Charney model subjected to localized time-periodic forcing manifests itself as a wavetrain that oscillates at the source frequency and amplifies in space with distance from the source; analytical and numerical results describing the salient characteristics of such waves are presented. The spatially amplifying disturbance is a hitherto unsuspected part of the response to a pulsating source, and coexists with the more familiar neutral Rossby wavetrains; it is likely to play a role in a wide range of atmospheric and oceanic phenomena.

The central results rely on a careful application of a causality criterion due to Briggs. These results illustrate a practical means of attacking spatial instability problems, which can be applied to a broad class of systems besides the one at hand. We have found that the Charney problem with positive vertical shear is not absolutely unstable, so long as the wind at the ground is non-negative. This implies that spatial instability and forced stationary-wave problems are well posed in an open domain under typical atmospheric circumstances.

The amplifying waves appear on the downstream side of the source, have eastward (downstream) phase propagation and have wavelengths that increase monotonically with decreasing frequency, becoming infinite at zero frequency. When the surface wind is not too large, the spatial amplification rate has a single maximum near the frequency $\omega_m = (f/N)\,U_z$, where f is the Coriolis parameter, N is the stability frequency and U_z is the vertical shear; the rate approaches zero at zero frequency and asymptotes algebraically to zero at large frequency for any positive surface wind. Distinct Charney and Green modes do not appear until the surface wind is made very large. The amplification rate at ω_m becomes infinite as surface wind approaches zero, suggesting a mechanism for the concentration of eddy activity.

We also discuss the relationship of these results to the structure of low- and high-frequency atmospheric variability.

1. Introduction

Considerable success has been achieved recently in understanding certain quasi-stationary circulation patterns of the Earth's atmosphere in terms of forced stationary Rossby wavetrains (Hoskins & Karoly 1981). This work has shown that the periodic boundary condition formally necessary on a sphere plays little role in the phenomena, as the waves do not have time to complete a circuit of the globe before they are damped out. For the purposes of theoretical work, it is therefore profitable to view the motions as existing in an open domain. Since the programme has been so successful in the zero-frequency case, it is likely to yield interesting

insights at low frequencies as well. Indeed, the atmospheric convection thought to be responsible for the forcing of the wavetrains is known to exhibit considerable fluctuation on timescales of five days or longer (Sardesmukh & Hoskins 1985). Interesting patterns have been discerned in the atmospheric low-frequency variability (Blackmon, Lee & Wallace 1984*a*; Blackmon *et al.* 1984*b*), and it has been found that such motions contribute significantly to the rectified eddy fluxes which partly determine the long term state of the atmosphere (Plumb 1986). However, study of the response to fluctuating forcing is hampered by the following uncertainty: the real vertically sheared atmosphere is unstable to baroclinic disturbances, and it seems likely that fluctuating forcing (even of bounded amplitude) will excite these disturbances in addition to trains of neutral Rossby waves. If the baroclinic disturbances grow locally in time, they may dominate the forced response and render it meaningless. Such a criticism has occasionally been levelled at the zero-frequency case as well: we shall see that in both cases, the criticism is nugatory. These questions have led us to the consideration of the circumstances in which the baroclinic instability manifests itself as a train of waves periodic in time but amplifying *in space* with distance from an oscillating source. Clarification of the nature of spatial baroclinic instability is the prime goal of this paper. Although the present study was motivated primarily by low-frequency phenomena, spatial baroclinic instability is of relevance to a broad range of features of the natural world; it has been considered in an oceanographic context by Thacker (1976), and we shall see that it can play a role in determining the distribution of atmospheric cyclogenesis. Accordingly, we have attempted to provide a complete portrait of the dependence on frequency and other physical parameters.

Disturbances that amplify in space rather than time arise in a variety of fluid-mechanical problems. Spatial instability has been treated for the case of viscous boundary layers by Gaster (1965), for free shear layers by Michalke (1965) and for jets and wakes by Betchov & Criminale (1966). Nevertheless, it is fair to say that the spatial problem has received far less attention than the temporal problem. Solution of the spatial problem is beset by a number of difficulties, not the least of which is the necessity of distinguishing roots representing amplifying disturbances from those representing evanescence. The means of resolving this question through application of causality are reviewed in §3. The simplest formulation of the causality condition is due to Briggs (1964), where the reader can also find a discussion of earlier approaches. A causality condition was imposed by Gaster (1965), who independently arrived at a formulation similar to that of Briggs. Recently, the free shear layer has been reexamined in the light of causality by Huerre & Monkewitz (1985). Briggs' criterion is simple to state, but fiendishly difficult to apply to all but the most elementary dispersion relations. A secondary purpose of the work presented here is to illustrate a strategy for implementation of the criterion in problems of realistic complexity.

In the geophysical context, the only complete treatment of spatial baroclinic instability is the work of Thacker (1976) on the two-layer model; however, this model suffers from many well-known deficiencies as a model of instability in a continuously stratified fluid. Hogg (1976) considered spatial modes in a continuous model, but restricted attention to a special profile with vanishing shear at the boundaries, which renders the results inapplicable to the atmosphere; moreover, Hogg did not make use of a causality condition. In the present work we consider spatial instability in the more realistic Charney problem (Charney 1947), paying special attention to the proper incorporation of causality. The problem also merits attention because the

application of Briggs' criterion determines whether the flow is absolutely unstable. We shall show that previous indications of absolute instability in the Charney problem with non-negative surface wind (Farrell 1982, 1983) are incorrect. It is because of the lack of absolute instability that forced wave problems in this baroclinic flow can be expected to yield physically meaningful results.

The plan of the paper is as follows. In §2 we review the required equations of motion and the formulation of the Charney problem. The means of incorporation of causality and their application to the Charney profile are discussed in §3. Asymptotic properties of the spatial instability in a number of limits are given in §4, while numerical results covering a broader range of parameter space are given in §5. Some (speculative) applications to understanding atmospheric variability are presented in §6. Our principal conclusions, along with some directions for future work, are summarized in §7.

2. Equations of motion

The baroclinic-instability problem studied in the seminal work of Charney (1947) is obtained by linearizing the quasigeostrophic β-plane equations about an isothermal atmosphere with constant vertical wind shear. Adopting a local Cartesian coordinate system with x pointing eastward, y northward and z upward, the potential-vorticity equation reads

$$\partial_t q + \mathrm{J}(\psi, q) = 0, \tag{2.1a}$$

$$q = \nabla^2\psi + \rho^{-1}\partial_z(\rho f^2/N^2)\,\partial_z\psi + \beta y, \tag{2.1b}$$

where ψ is the stream function in the (x, y)-plane, ∇^2 is the horizontal Laplacian, $\mathrm{J}(A, B) = \partial_x A\,\partial_y B - \partial_x B\,\partial_y A$, $\rho(z)$ is the background density, f is the (constant) Coriolis parameter at the central latitude, N is the Brunt–Väisälä frequency and β is the meridional gradient of the Coriolis parameter. For an isothermal atmosphere $\rho = \rho_0 \exp(-z/H)$, where $H = RT/g$ is the scale height, and N is constant. For a flat frictionless lower boundary, the bottom boundary condition is

$$\partial_t\partial_z\psi + \mathrm{J}(\psi, \partial_z\psi) = 0 \quad \text{at } z = 0, \tag{2.1c}$$

and the system is closed by application of a radiation or boundedness condition at $z = \infty$. Henceforth we shall adopt non-dimensional units with depth scaled by H, length by the radius of deformation $L_\mathrm{d} = NH/f$, and velocities by $U_z H$, where U_z is the vertical shear of the basic state. We substitute

$$\psi = -(U_0 + z)\,y + \Phi(z)\,\mathrm{e}^{\mathrm{i}(kx+ly-\omega t)}. \tag{2.2}$$

where U_0 is the non-dimensional surface wind, into (2.1) and linearize to obtain the problem

$$\frac{\mathrm{d}^2\Phi}{\mathrm{d}z^2} - \frac{\mathrm{d}\Phi}{\mathrm{d}z} + \left[\frac{1+\beta}{U_0 - \omega/k + z} - (k^2 + l^2)\right]\Phi = 0, \tag{2.3a}$$

$$\frac{\mathrm{d}\Phi}{\mathrm{d}z} - \frac{\Phi}{U_0 - \omega/k} = 0 \quad \text{at } z = 0, \tag{2.3b}$$

which is completed by an energy-decay condition

$$\Phi\,\mathrm{e}^{-\frac{1}{2}z} \to 0 \quad \text{as } z \to \infty. \tag{2.3c}$$

These equations define the dispersion relation Δ such that k, l and ω are related by $\Delta(k, l, \omega) = 0$. Specifically, if $\phi(z, k, l, \omega)$ is the solution to (2.3a) satisfying (2.3c), then (2.3b) implies

$$\Delta = \left[\frac{\mathrm{d}\phi}{\mathrm{d}z} - \frac{\phi}{U_0 - \omega/k}\right]_{z=0}. \tag{2.4}$$

U_0 and β are the fundamental parameters of the problem; in terms of the dimensional quantities, they are given by $U_0 = (U_0)_{\rm dim}/U_z H$ and $\beta = \beta_{\rm dim} L_{\rm d}^2/U_z H$. The properties of the temporal problem $\omega(k, l)$ have been exhaustively studied, and are summarized in Pedlosky (1979). In the temporal problem, U_0 simply shifts the real part of ω, and hence can be set equal to zero without loss of generality. Then, if n is the greatest integer less than or equal to β, there is a unique unstable mode at each k^2+l^2, except when k^2+l^2 is equal to zero or any of $n+1$ critical values; $\omega \to 0$ at these points. For typical values of the atmospheric shear, β lies between zero and one, whence there is a single non-zero critical wavenumber k_c.

For the most part we shall concentrate on motions that amplify in the x-direction only. In this case l is a specified real number and k is the unknown (complex) quantity to be determined. Some results on the more general problem involving amplification in both directions are offered in §5.

In the numerical results presented below, Δ was computed by numerically solving (2.3a) subject to (2.3c) and making use of (2.4). A fourth-order variable-step method was used, and (2.3c) was applied by matching the solution to the decaying exponential solution at $z = 10$. Typically, an increment $\delta z = 0.1$ near $z = 0$ was sufficient to yield an accuracy of two significant figures in the final results. The equation $\Delta = 0$ was solved for k using Newton's method along a continuation path to be described in §3. It is evident from (2.3) that if (k, l) is a solution corresponding to ω then $(-k^*, -l^*)$ is a solution corresponding to $-\omega^*$; hence it suffices to consider only $\mathrm{Re}\,(\omega) > 0$.

3. Evolution of image of the Bromwich contour

3.1. *Statement of Briggs' criterion*

Solution of the dispersion relation for k in terms of real ω generally yields many roots with non-zero imaginary part, and the chief difficulty arises in discriminating between spatially amplifying and evanescent disturbances. This is accomplished by identifying those solutions that can be obtained from an initial-value problem with spatially bounded initial data. The means of extracting causality information from the dispersion relation is discussed in Briggs (1964); as the clarity of his exposition could hardly be improved upon, the reader is referred there for a complete account and historical review. This material has also been reviewed in Merkine (1977) and Huerre & Monkewitz (1985). Here we shall provide only the background needed to state the result.

For the purpose of illustration, consider a one-dimensional constant coefficient linear operator $\mathrm{L}(\partial_t, \partial_x)$ defined on the domain $x \in [-\infty, \infty]$. Let $\mathrm{L}\, \mathrm{e}^{\mathrm{i}(kx-\omega t)} = \Delta(k, \omega)\, \mathrm{e}^{\mathrm{i}(kx-\omega t)}$, so that $\Delta(k, \omega) = 0$ defines the dispersion relation. Then, by making use of the Laplace transform in time and the Fourier transform in space, the solution to the forced initial-value problem

$$\mathrm{L}\psi(x, t) = F(x, t), \quad \psi(x, 0) = \psi_0(x) \tag{3.1}$$

is found to be

$$\psi(x, t) = \int_{-\infty+\mathrm{i}\gamma}^{\infty+\mathrm{i}\gamma} \mathrm{d}\omega \int_{-\infty}^{\infty} \mathrm{d}k \frac{G(k, \omega)\, \mathrm{e}^{\mathrm{i}(kx-\omega t)}}{\Delta(k, \omega)}, \tag{3.2}$$

where γ is required to be larger than the maximum growth rate $\mathrm{Im}\,(\omega(k))$ over all real k. $G(k, \omega)$ is determined by the forcing and initial conditions; considered as a function of ω, it may have poles on the real ω axis corresponding to spikes in the spectrum of the forcing, but is required to be analytic in the upper-half ω-plane. The

path of integration in ω is known as the 'Bromwich contour'; we evaluate the long-time asymptotics of (3.2) by moving the Bromwich contour as far as possible toward the real ω-axis. For a given ω, the integrand has poles where $\Delta(k,\omega)=0$, i.e. at $k=k(\omega)$, where $k(\omega)$ is generally multiple-valued. For any γ, $k(\omega_r+i\gamma)$ as ω_r ranges over all real values defines a set of curves, which we shall refer to as images of the Bromwich contour under the mapping $k(\omega)$, or simply 'Bromwich images'. For the original γ, none of the Bromwich images cross the real k-axis, and so (3.2) receives contributions only from spatially evanescent solutions. However, as γ is reduced to zero, one or more of the Bromwich images may cross the real k-axis, requiring the path of k-integration to be deformed so as to avoid the singularity. If the crossing is from above, (3.2) will receive contributions from negative Im (k) when $x>0$, which represent spatially amplifying disturbances. If poles cross from below, amplifying disturbances are found for $x<0$. Thus it is the poles $k(\omega)$ that cross the real k-axis as $\gamma\to 0$ that represent spatial instabilities.

It may happen that as γ is reduced toward zero, two branches of $k(\omega)$ *that originated on opposite sides of the real k-axis for the original choice of* γ coalesce for some ω on the Bromwich contour. In this case, the contour of integration for k cannot be deformed so as to avoid the singularity, and it can be shown that the contribution from this singularity grows exponentially in time at any fixed x. Such systems are said to be 'absolutely unstable'. The necessity of the two roots coalescing at the saddle point having originated on opposite sides of the real axis is an important part of the absolute instability criterion, which has not always been sufficiently emphasized. The situation in which a system is unstable but not absolutely unstable is known as 'convective instability'; it is only for convectively unstable systems that the spatial instability problem is well posed, though in cases where the absolute instability is weak, the spatial modes may nevertheless be of physical interest. We shall see shortly that the Charney problem is convectively unstable for any $U_0\geqslant 0$.

We note in passing that if the pinch occurs *on* the real ω-axis then *algebraic* growth in time is possible if the spectrum of the forcing has a pole at the value ω_0 where the pinch occurs. This is so because the residue $[\partial_k \Delta(k(\omega),\omega)]^{-1}$ has a pole at ω_0, which leads to a double pole in the integrand if G also has a pole at ω_0. Since $\mathrm{d}\omega/\mathrm{d}k=0$ at a pinch, this state of affairs corresponds to forcing of a wave with zero group velocity; the energy accumulates because it cannot propagate away from the source. Such flows are not convectively unstable in the technical sense, because the perturbations grow in time at a fixed site; in a generalized sense, though, the problem may still be regarded as convective, in that the temporal growth is dependent on continuation of the forcing and would disappear if the forcing were shut off. It can be inferred from the results of Held, Panetta & Pierrehumbert (1985) and Held, Pierrehumbert & Panetta (1986) that zero-group-velocity modes with real ω do not occur on the Rossby-wave branch of the Charney dispersion relation when $l=0$ (see especially figure 1 of Held *et al.* 1986). However, such modes can certainly exist when $l\neq 0$, just as they do in the barotropic case. The resonant forcing of Rossby waves with zero group velocity is a distinct issue from baroclinic instability, and will not be taken up further. Merkine (1982) has discussed zero-group-velocity resonances of barotropic Rossby waves; his discussion fully illuminates the basic issues.

It is straightforward to extend the causality analysis to the case in which the evolution is governed by a multidimensional partial differential equation with non-constant coefficients in some direction (other than x and t), such as arises in the study of baroclinic instability. Since a nearly identical initial value problem problem was treated exhaustively by Huerre & Monkewitz (1985), we shall present only a

sketch of the solution here. Consider forced y-independent motions of the quasi-geostrophic system (2.1). If one adds a vorticity source $F(x,t)\,\delta(z-z')$ to the right-hand side of (2.1a) and linearizes about the Charney profile one obtains

$$(\partial_t + U\,\partial_x)\,q' + (1+\beta)\,\partial_x \psi' = F(x,t)\,\delta(z-z'), \tag{3.3}$$

where $U \equiv U_0 + z$ and $q' = \partial_{xx}\psi' - \partial_z \psi' + \partial_{zz}\psi'$. The boundary conditions at $z = 0$ and $z = \infty$ are the same as for the homogeneous problem. Taking the Fourier transform in x and the Laplace transform in time, we find that the Fourier–Laplace transform of ψ' is determined by the linear inhomogeneous problem

$$\frac{\mathrm{d}^2\Phi}{\mathrm{d}z^2} - \frac{\mathrm{d}\Phi}{\mathrm{d}z} + \left[\frac{1+\beta}{U-\omega/k} - k^2\right]\Phi = \frac{G(k,\omega)\,\delta(z-z')}{-\mathrm{i}\omega + \mathrm{i}kU}, \tag{3.4}$$

where $\Phi(k,\omega,z)$ is the Fourier–Laplace transform of ψ' and $G(k,\omega)$ is the transform of F. The boundary conditions on Φ are still (2.3b, c). The solution to this problem can be constructed from solutions to the homogeneous equation (2.3) using elementary methods. We find that

$$\Phi(k,\omega,z) = \frac{G(k,\omega)}{(-\mathrm{i}\omega + \mathrm{i}kU(z'))\,W(k,\omega,z)} \begin{cases} \Phi_+(z)\,\Phi_-(z') & (z > z'), \\ \Phi_+(z')\,\Phi_-(z) & (z < z'), \end{cases} \tag{3.5}$$

in which Φ_+ is a solution to (2.3) satisfying the upper boundary condition and Φ_- is a solution satisfying the lower boundary condition. $W(k,\omega,z)$ is the Wronskian $[\Phi_+\,\partial_z\Phi_- - \Phi_-\,\partial_z\Phi_+]$ of Φ_+ and Φ_- evaluated at z'; from the differential equation (2.3) it is evident that

$$W(k,\omega,z) = W(k,\omega,0)\,\mathrm{e}^z \equiv W_0(k,\omega)\,\mathrm{e}^z. \tag{3.6}$$

Note that W vanishes identically precisely when Φ_+ and Φ_- are proportional, i.e. when there is a solution to the homogeneous problem. Thus $W_0(k,\omega)$ plays the same role as the polynomial $\Delta(k,\omega)$ appearing in (3.2), and in fact is proportional to the dispersion relation Δ as defined in (2.4).

Most of our discussion of Briggs' criterion remains unchanged, save that Δ becomes a general analytic function rather than a polynomial. There are two new wrinkles: (a) Φ has an additional pole where $-\mathrm{i}\omega + \mathrm{i}kU(z') = 0$, and ($b$) for any real constant C in the range of U, Φ has a branch point where $\omega/k = C$ correspondng to a continuum mode. The Bromwich image $k(\omega)$ for each continuum mode $k = \omega/C$ is a line parallel to the real k-axis; because it does not cross the axis it does not contribute to spatial instability. The same argument applies to the pole at $k = \omega/U(z')$. If the forcing has a pole at $\omega = 0$, higher-order singularities can arise from the vanishing of the term $\omega - kU$ at $\omega = k = 0$; treatment of these singularities can be avoided by working with the transform of the meridional velocity, which is simply $\mathrm{i}k\Phi$ and has no problematic behaviour at $k = 0$.

3.2. *Application to the Charney problem*

Application of the Briggs criterion requires examination of the family of curves $k(\omega_\mathrm{r} + \mathrm{i}\gamma)$, where ω_r ranges over all real values and γ parametrizes the family. The large number of branches of $k(\omega)$ might at first make the task seem daunting; however, the difficulty is mitigated by the fact that one need only consider branches that cross the real k-axis. For any given γ, the crossing points can be determined by inspection of the function $\omega(k)$ on the real k-axis; one simply identifies the values k_0 at which $\omega_\mathrm{i}(k_0) = \gamma$, whence the corresponding $\omega_\mathrm{r}(k_0)$ at the crossings are known. With a solution $k(\omega_\mathrm{r} + \mathrm{i}\gamma)$ for a particular ω_r in hand, the values of k for a range of

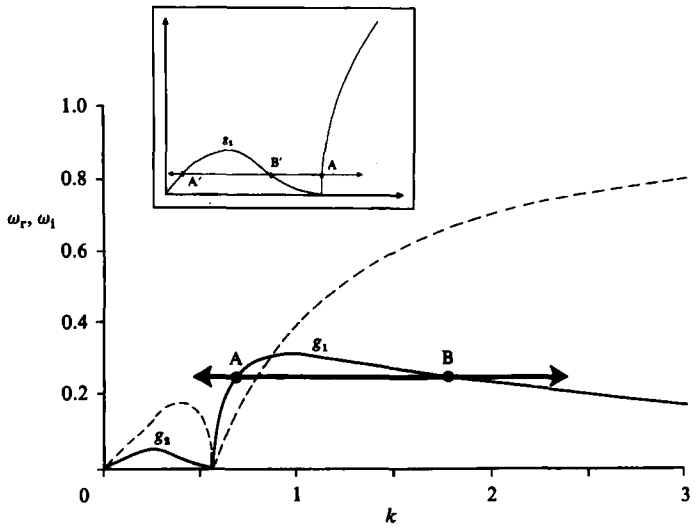

FIGURE 1. Complex frequency ω as a function of real wavenumber k for the Charney problem with $\beta = 0.5$, $U_0 = 0$ and $l = 0$. The growth rate $\mathrm{Im}(\omega)$ is given by the solid curve, while the frequency $\mathrm{Re}(\omega)$ is given by the dashed curve. g_1 is the maximum growth rate of the Charney-mode branch while g_2 is that for the Green-mode branch. The points A and B indicate the intersection of the line $\mathrm{Im}(\omega) = g$ with the Charney branch, for $g_2 < g < g_1$. The inset shows a magnification of the long-wave behaviour, indicating the disposition of the intersection points A′ and B′ with the Green-mode branch when $g < g_2$. For further details see text.

ω_r can be determined numerically by continuation methods. This strategy exploits information from the familiar temporal problem to facilitate solution of the more difficult spatial problem. For complicated or unexplored systems such a scheme is essential, as $\omega(k)$ can always be reliably determined without *a priori* information by use of globally convergent eigenvalue routines, whereas $k(\omega)$ cannot.

Figure 1 shows $\omega(k)$ for the Charney problem with $\beta = 0.5$, $l = 0$ and $U_0 = 0$. The eigenvalue ω vanishes at $k = 0$ and $k = k_c = 0.5(\beta(\beta+2))^{\frac{1}{2}} \approx 0.56$; the weakly growing modes to the left of k_c are known as the 'Green modes', while the strongly growing modes to the right are known as the 'Charney modes'. At large k, $\omega_i \to 0$ and $\omega_r \to 1$ monotonically with $O(1/k)$ error (see Appendix B). Let g_1 be the maximum Charney-mode growth rate and g_2 be the maximum Green-mode growth rate. When $\gamma > g_1$ none of the Bromwich images cross the real k-axis. Now consider what happens as γ is reduced. When $g_2 > \gamma > g_1$ the line $\omega_i = \gamma$ intersects $\omega_i(k)$ at two points (marked A and B in figure 1), and consequently the Bromwich image crosses the real k-axis at the values of k_r corresponding to A and B. To determine the behaviour near a point $k_1 \in \mathbb{R}$, we form the expansion

$$\omega(k) = \omega(k_1) + (k-k_1)\,\omega'(k_1) + \tfrac{1}{2}(k-k_1)^2\,\omega''(k_1) + \ldots \tag{3.7}$$

and solve for $k-k_1$ to obtain

$$k-k_1 = \frac{\omega-\omega(k_1)}{\omega'} - \frac{1}{2}\frac{(\omega-\omega(k_1))^2\,\omega''}{\omega'^3} + \ldots, \tag{3.8}$$

in which ω is to be varied along the Bromwich contour. Suppose $\gamma = g_1 + \mathrm{i}\delta$ with $\delta \ll 1$, and k_1 is chosen such that $\mathrm{Im}(\omega(k_1)) = g_1$. Then $\omega - \omega(k_1) = (\omega_r - \omega_r(k_1)) + \mathrm{i}\delta$, $\omega'(k_1)$ is real and $\mathrm{Im}(\omega''(k_1))$ is negative. Consequently, as ω_r is

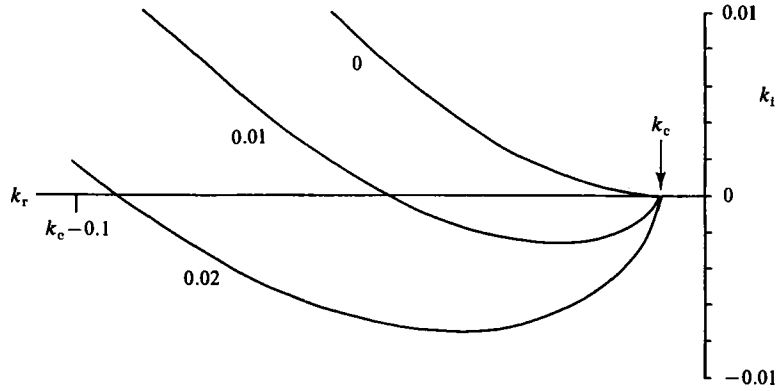

FIGURE 2. Behaviour of Bromwich images $k(\omega_r+i\gamma)$ near the critical point k_c, as determined by the asymptotic results. The value of γ is indicated on each curve. ω_r varies from zero (at the rightmost terminus of each curve) to a small positive value. Parameters are as for figure 1.

varied, (3.8) describes a parabola in the k-plane which crosses the real k-axis at two points near k_1 when $\delta < 0$. The orientation of the parabola is determined by the sign of $\omega'(k_1)$; in the problem at hand, $\omega'(k_1) > 0$, the parabola opens upward, and therefore the Bromwich image crosses the real axis *from above*. This implies that the spatial instabilities connected with this branch amplify in the positive x-direction, a result that is consonant with the intuitive notion that the disturbances should amplify in the direction of the group velocity of the most unstable mode.

If k_1 is not near the growth-rate maximum, $\mathrm{Im}\,(\omega'(k_1)) \neq 0$ and only the first term in (3.8) is needed. As $\omega_r - \omega_r(k_1)$ is increased through zero, k crosses the real axis from above if $\mathrm{Im}\,(\omega'(k_1)) > 0$ and from below if $\mathrm{Im}\,(\omega'(k_1)) < 0$. Hence the Bromwich image crosses from above at A and crosses back from below at B. We have no information about the form of the curve between A and B; although it started as a parabola for $\gamma \approx g_1$, its topology may change as γ is reduced. We shall see shortly that this indeed occurs.

As γ is reduced below g_2, a second loop of the Bromwich image crosses the real k-axis, intersecting it at points A′ and B′ to the left and right of the Green-mode maximum. Since $\omega' > 0$ at this maximum, the crossing is from above, just as for the Charney mode. As γ is reduced to zero, A′ moves to $k_r = 0$, B moves to $k_r = \infty$, and B′ and A converge on k_c from opposite sides.

Let us now consider the behaviour of the Bromwich image near k_c as $\gamma \to 0$. In Appendix A it is shown that in the vicinity of any neutral point

$$k - k_c = -B_1 \Omega^2 - B_2 \Omega^3 + iB_3 \Omega^4 + \ldots, \tag{3.9}$$

where B_1, B_2 and B_3 are positive real constants (provided $U_0 > 0$) and Ω is proportional to ω with a positive constant of proportionality. Let $\Omega = \Omega_r + i\delta$, with $\delta > 0$. The curve begins above the real k-axis at $\Omega_r = 0$; when $\Omega_r \approx (B_2/2B_1)\,\delta^2$ it crosses the axis at $k \approx k_c + B_1\,\delta^2$ (point A in figure 1), and when $\Omega_r \approx (2B_1\,\delta/B_3)^{\frac{1}{3}}$ it crosses back at $k \approx k_c - B_1(2B_1\,\delta/B_3)^{\frac{2}{3}}$ (point B′ in figure 1). Asymptotic curves $k(\omega)$ for $\beta = 0.5$ and $\gamma = 0.02$, 0.01 and 0 are shown in figure 2. The principal inference from this calculation is that points A and B′ are connected by a continuous curve when γ is small, though at larger γ A connects with B while A′ connects with B′. Hence, as the Bromwich contour is moved towards the real axis, the Bromwich image associated with the Green modes must at some point coalesce with that associated

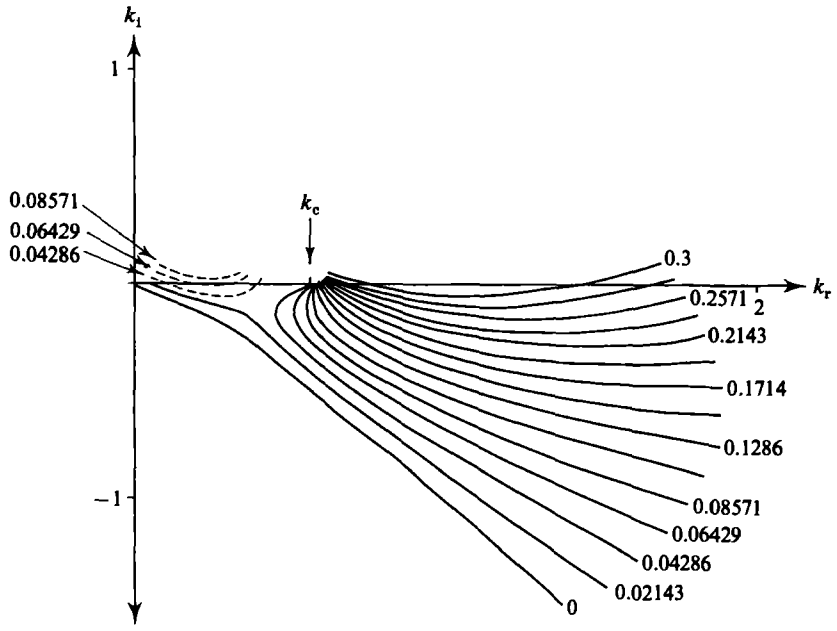

FIGURE 3. Numerically determined development of the Bromwich images. Dashed curve gives segment associated with Green modes for $\omega_r \in [0, 0.2]$; Solid curve gives segment associated with Charney modes for $\omega_r \in [0, \frac{2}{3}]$. Values of γ are indicated on each curve. Parameters are as for figure 1.

with the Charney modes; past this point the curve breaks, and A connects with B′ while A′ connects with B. When $\gamma = 0$ the arc emanating from k_c lies entirely above the real k-axis and does not lead to spatial instability. One expects a single continuous branch of spatial instability continuing from the point $k = 0, \omega = 0$.

This picture is confirmed by the numerically computed Bromwich images. In figure 3 we show the evolution of these images as γ (noted on each curve) is reduced to zero. The Green-mode branch (dashed curves) is shown for the range $\omega_r \in [0, 2]$, while the Charney-mode branch (solid curves) is shown for the range $\omega_r \in [0, \frac{2}{3}]$; in both cases the leftmost point on each curve is the mapping of $\omega = 0 + i\gamma$. As anticipated, the two branches coalesce as γ is reduced, the coalescence occurring between $\gamma = 0.04286$ and $\gamma = 0.02143$. At this point the curves break and rejoin, so that when $\gamma = 0$ we are left with a single spatially amplifying branch on which k_i is monotonic in ω. (The loop corresponding to the asymptotic results in figure 2 is not shown.) The only relic of the Green-mode/Charney-mode distinction is a slight kink in the low-frequency segment of the curve.

It is important to note that the coalescence is between roots that originated *on the same side* of the real k-axis. Hence the system under consideration is not absolutely unstable; the asymptotic results suggest that this is the case for all positive β and U_0, and we have encountered no numerical evidence to the contrary.

In contrast, Farrell (1982, 1983) concluded that for a range of $U_0 \geqslant 0$, there is an absolute instability associated with the Green modes. The use in his work of a WKB approximation to the true dispersion relation does not account for the differing conclusion; from the dashed contours in figure 4(*b*) of Farrell (1982), computed for $\beta = 1$ using the WKB approximation, one can infer a development of the Bromwich image much the same as in our figure 3. Farrell simply failed to note the rather subtle

fact that the saddle point shown in his figure joins two branches which originated on the same side of the real k-axis, and hence does not represent absolute instability. This underscores the importance of a thorough examination of the topology of the Bromwich images. It is not sufficient merely to search for saddle points in the unstable portion of the complex plane.

4. Asymptotic results on $k(\omega)$

4.1. *Low-frequency behaviour*

The spatial amplification rate for low-frequency forcing can be obtained from the long-wave form of the dispersion relation. Since ω enters (2.3) only in the combination $U_0 - c$, where $c \equiv \omega/k$, the long-wave behaviour is determined by the value of c corresponding to $k = 0$ and $U_0 = 0$; we shall call this value $c_0(\beta, l)$. c_0 is generally complex and non-zero. For small k, ω then has the behaviour $\omega = (U_0 + c_0)k$, whence

$$k = \frac{c_{0r} + U_0 - ic_{0i}}{(c_{0r} + U_0)^2 + c_{0i}^2}\omega, \tag{4.1}$$

The temporally unstable branch has $c_{0i} > 0$, and leads to a spatial instability that amplifies in the positive x-direction. The amplification rate is linear in ω and decreases monotonically with increasing U_0.

In the special circumstances in which $k = 0$ is a critical point (e.g. when $l = 0$ and β is an integer) c_0 vanishes and the above discussion must be modified. In Appendix A it is shown that in this case

$$k = \begin{cases} \dfrac{\omega}{U_0} - iD\left(\dfrac{\omega}{U_0}\right)^2 & (U_0 > 0), \qquad (4.2a) \\[2ex] (1-i)\left(\dfrac{\omega}{2D}\right)^{\frac{1}{2}} & (U_0 = 0), \qquad (4.2b) \end{cases}$$

where D is a positive real constant. In both cases the amplification is again in the positive x-direction. As U_0 approaches zero the domain of frequencies in which (4.2a) is valid collapses to zero, and (4.2b) applies. For positive U_0 the long-wave amplification rates for fixed small ω are weak compared with the non-critical case simply because the temporal growth rates become weak when $k = 0$ is a critical point. When $U_0 = 0$ the weak temporal growth rates are offset by very slow propagation, leading to an amplification rate that is greater than that of the non-critical case.

4.2. *Behaviour at large U_0*

When k_i is small and ω is differentiable the amplification rate can be recovered from data on the real k-axis by means of the expansion

$$\omega(k_r + ik_i) = \omega(k_r) + ik_i\omega'(k_r), \tag{4.3}$$

in which $\omega(k_r + ik_i) \equiv \omega$ is required to be real. Matching real and imaginary parts of (4.3) implies

$$\omega_r(k_r) = \omega + O(k_i), \tag{4.4a}$$

$$k_i = -\frac{\omega_i(k_r)}{\omega_r'(k_r)}. \tag{4.4b}$$

Equation (4.4a) determines k_r, which may then be used in (4.4b); this is the familiar group-velocity transformation (Gaster 1962).

If U_0 is large and k_r is not a critical point then $\omega_r(k_r) \approx U_0 k_r$ and $\omega_r'(k_r) \approx U_0$, whence

$$k_i = -\frac{\omega_i(\omega/U_0)}{U_0}. \tag{4.5}$$

Thus, apart from rescaling by $-1/U_0$, the graph of spatial amplification rate becomes identical to that of the temporal growth rate evaluated at $k_r = \omega/U_0$; in particular, the value of ω yielding the maximum amplification rate increases linearly with U_0. This formula becomes invalid when ω/U_0 is near a critical point k_c, where the derivative of $\omega(k)$ becomes infinite. It will be seen in §5 that the large-U_0 behaviour does not begin to be realized near k_c until the surface wind is unphysically large; hence the detailed behaviour near k_c will not be pursued. Away from critical points, the asymptotic behaviour is approached at more moderate values of U_0, and the formula is correspondingly more useful.

4.3. *Short-wave behaviour*

The large-k asymptotic form of $\omega(k)$ can be used to infer the behaviour of $k(\omega)$ for values of ω such that $k \gg 1$. In order to shed some light on the circumstances in which k is expected to be large, let us first examine the function $\omega(k)$ for $U_0 = 0$. Recall that $\omega_r = 1 + O(1/k)$ and $\omega_i = O(1/k)$ at large real k in this case, which suggests that k becomes infinite as $\omega \to 1$. Moreover, the group velocity $\mathrm{d}\omega_r/\mathrm{d}k$ is $O(1/k^2)$ at large k, in consequence of which the estimated spatial amplification rate $-\omega_i/(\mathrm{d}\omega_r/\mathrm{d}k)$ becomes infinite at large k. Thus short waves propagate so slowly that they are expected to lead to infinite spatial amplification rates even though their temporal growth rates are small. On the other hand, if $U_0 > 0$, then $\omega \approx 1 + U_0 k$ at large k, whence $k_r \approx \omega/U_0$ for $\omega \gg U_0$; further, $\mathrm{d}\omega_r/\mathrm{d}k \approx U_0$ and $k_i \approx -\omega_i/U_0$ vanishes like $O(1/\omega)$ for very large ω. These considerations suggest that when U_0 is not too large, k_r and k_i become large near $\omega = 1$, and k_i falls to zero as ω is made much larger. A proof of this assertion proceeds from the large-k asymptotic dispersion relation discussed in Appendix B. It is shown there that

$$k = \{(\omega-1) + [(\omega-1)^2 - 4U_0 b]^{\frac{1}{2}}\}/2U_0, \tag{4.6}$$

where b is a complex constant with negative real and positive imaginary part, given in (B 9). Equation (4.6) is valid only when it predicts $k \gg 1$. As expected, $k_i = O(1/\omega)$ at large ω. For $U_0 = 0$ and $\omega < 1$, (4.6) reduces to $k = b/(\omega-1)$, whence $k_r \to +\infty$ and $k_i \to -\infty$ as $\omega \to 1$ from below. Values of ω greater than unity do not lead to spatial instability in this case. When U_0 is small but non-zero, (4.6) is valid when ω is of order unity or larger and predicts that $-k_i$ attains a maximum value proportional to $U_0^{-\frac{1}{2}}$ at $\omega = 1$. Because of the square root in the numerator of (4.6), the peak in the amplificatiion rate is not expected to be sharp. When U_0 is of order unity or larger, (4.6) is not valid unless ω is large, and the predicted peak in amplification rate at $\omega = 1$ is spurious.

Numerical determinations of $k_i(\omega)$ with $\beta = 0.5$ and $l = 0$ are shown in figure 4 for the cases $U_0 = 0$ and $U_0 = 0.2$, along with the corresponding asymptotic predictions of (4.6). In both cases the behaviour of the numerical results begins to conform with the asymptotic formula at moderate values of ω. In particular, for the case $U_0 = 0.2$ the broad maximum in the amplification-rate curve near $\omega = 1$ is quite well reproduced by (4.6). (This is to be expected, as k_r becomes large for $\omega \approx 1$, even though k_i remains bounded.) Another noteworthy feature of the results is the great sensitivity of the response curve to modest changes of U_0; this, of course, stems from the $\omega = 1$ singularity appearing in the limit of vanishing surface wind.

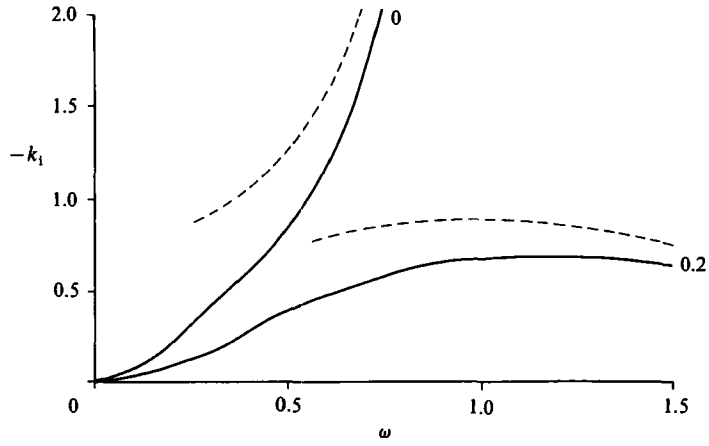

FIGURE 4. Amplification rate $-k_i$ as a function of real ω, for $U_0 = 0$ and $U_0 = 0.2$ (other parameters as for figure 1). The numerical results are shown by solid curves, and the corresponding short-wave asymptotic results are shown by dashed curves.

The peak in amplification for unit frequency and the infinite amplification for $U_0 = 0$ are of great physical import. In consequence of the former, it would be expected that the variability of an atmosphere subjected to stochastic forcing would be concentrated in a broad band of frequencies disposed about $\omega = 1$, supposing the world to be linear; for $U_0 = 0.2$, e.g. there would be a strong preference for frequencies greater than 0.5. Nonlinearity, however, complicates the relation between amplification rate and response amplitude; in fact, the spectrum of fluctuations of 500 mb geopotential height in the atmosphere peaks at very *low* frequencies (Blackmon 1976). Allowing for nonlinearity, a more plausible prediction is that motions forced at frequencies near $\omega = 1$ saturate and lose coherence rather close to the source region, leading to a relatively local response. Low-frequency motions, in contrast, can propagate long distances from their source before being disrupted by nonlinear effects.

The singularity in amplification rate at $U_0 = 0$ has implications for the spatial distribution of variability. Other factors being equal, it implies that in a medium in which U_0 varies slowly in x and y, the greatest variability will be found in or somewhat downstream of regions of small U_0. The singular amplification rate is connected with the transition of the Charney modes to absolute instability at $U_0 = 0$. The reasoning here is similar to that found in the work of Landahl (1972), who made use of a more qualitative group-velocity argument in order to explain the appearance of spikes at certain points in boundary-layer flows. The success of these arguments in laboratory conditions lends confidence to the expectation that a similar mechanism operates in the atmosphere.

As the energy of short waves is trapped near to the lower boundary, these waves are apt to be strongly damped by Ekman friction. It is expected that Ekman friction, by stabilizing sufficiently short waves, would cause k_i to fall to zero at a finite frequency. For the case $U_0 = 0$, the high-frequency cutoff would occur at some $\omega < 1$ and the singularity in k_i would be eliminated in favour of a sharp peak at frequencies somewhat smaller than unity. Similarly, for small positive U_0, the very gradual decay of k_i at frequencies greater than unity would be replaced by a sharper cutoff and the peak response would be shifted to somewhat lower frequencies. Incorporation of

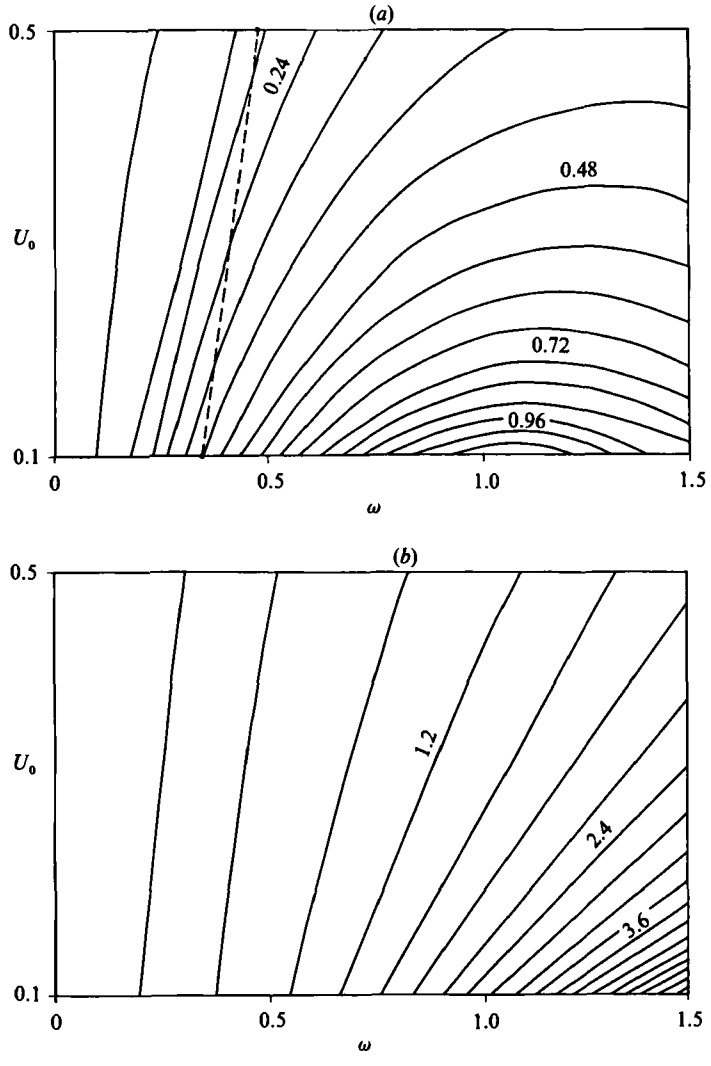

FIGURE 5. $k(\omega, U_0)$ for $\omega \in [0, 1.5]$ and $U_0 \in [0.1, 0.5]$, with $\beta = 0.5$ and $l = 0$: (*a*) Im (k) (all values negative); (*b*) Re (k) (all values positive). The dashed line gives the locus of the points where Re $(k) = k_c$.

Ekman friction into the results of Appendix B (and the numerical results) is entirely straightforward; however, in order to focus on the more basic features of the problem, a quantitative discussion of frictional effects will be left to future work.

5. Numerical results on $k(\omega, \beta, U_0)$

In this section we shall provide a more comprehensive picture of the dependence of k upon ω, β and U_0, as revealed by numerical calculations. Quantitative results will be presented only for the case $l = 0$, for which lines of constant phase are oriented perpendicular to the x-axis; we shall show later how certain characteristics of oblique waves can be recovered from these results. Consider first the dependence of k on ω and U_0 with β held fixed. Figure 5(*a*) shows contours of k_i in the (ω, U_0)-plane for

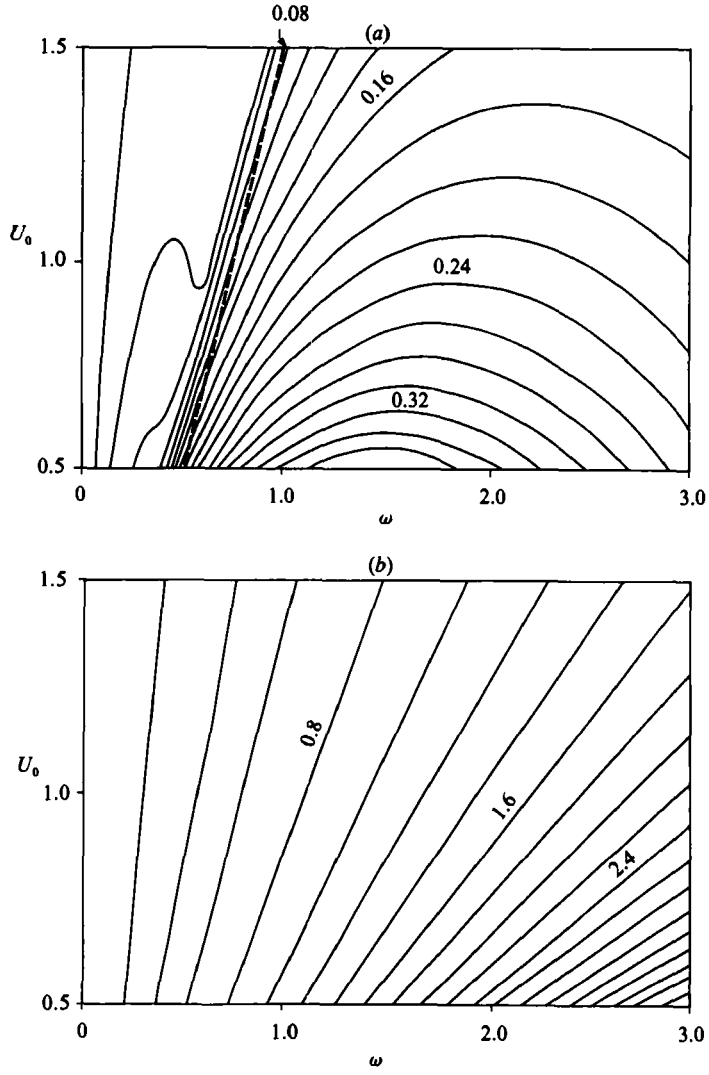

FIGURE 6. As for figure 5, except $\omega \in [0, 3.0]$ and $U_0 \in [0.5, 1.5]$.

$\omega \in [0, 1.5]$ and $U_0 \in [0.1, 0.5]$, with $\beta = 0.5$. In the range of U_0 shown, the amplification rate has only a single maximum as a function of ω; as predicted in §4.3, the peak occurs at $\omega = 1$ when U_0 is small. As U_0 is increased, the peak shifts gradually to higher frequencies, evidencing a behaviour qualitatively like the large-U_0 limit described in §4.2. Although there is no separate Green-mode maximum, a vestige of the Charney/Green distinction remains in the form of a band of low frequencies in which the amplification rates are small and increase weakly with increasing frequency. This feature is also evident in the curve for $U_0 = 0.2$ in figure 4, where it shows up as a kink in the amplification curve near $\omega = 0.25$. It is within the weakly unstable range that the low-frequency approximation of §4.1 is useful. The boundary of this regime shifts to higher frequencies as U_0 is increased. Despite the existence of this band, the amplification rate becomes appreciable at fairly low frequencies, provided the surface wind is not too large.

The corresponding results on k_r, shown in figure 5(*b*), reveal no features of

particularly striking interest, but are included for the sake of completeness. At all U_0 the real wavenumber is a monotonically increasing function of frequency. As predicted by asymptotics, the wavelengths become quite short near unit frequency when U_0 is made small. Recall that the radius of deformation has been used as the lengthscale. Hence the contour $k_r = 1.2$ can be thought of as separating the region of parameter space in which 'synoptic-scale' motions (with wavelength shorter than about 6 deformation radii) are generated from that in which the larger-scale motions typically associated with low-frequency atmospheric variability are generated.

The above results are extended to larger surface winds ($U_0 \in [0.5, 1.5]$) in figure 6. The peak amplification rate continues to move toward higher frequencies as U_0 is increased. Near $U_0 = 0.8$ the amplification rates cease being monotonic at low frequencies, and a dip forms separating low-frequency Green-mode from high-frequency Charney-mode behaviour. (This dip is not evident at higher U_0 in the figure, because the amplification rates are so small that few contours appear in the low frequency range.) According to the results of §4.2, it was inevitable that such a dip would appear, as the spatial results must come to resemble the temporal results at sufficiently large U_0. To emphasize the convergence to this limit, we have plotted as a dashed line in figure 6(*a*) the curve on which k_r is equal to the critical wavenumber k_c obtained from analysis of the temporal problem. It is seen that for values of U_0 greater than unity this curve accurately demarcates the frequency above which rapidly growing Charney modes are excited. It should be emphasized, though, that the values of U_0 in figure 6 are too large to be of much interest in the atmospheric context.

The dependence of k on β is of considerable interest, as β amounts to a non-dimensional measure of the strength of the basic-state shear, with large β corresponding to weak shear. Contours of k_i in the (ω, β)-plane with U_0 fixed at 0.2 are shown in figure 7. Surprisingly, the amplification rates are relatively insensitive to β. Values of k_r (not shown) are similarly insensitive to β. At the higher frequencies the amplification rate actually increases slightly with increasing β. Evidently, the weakening of temporal growth rates as the shear is reduced is entirely offset by the lower propagation speeds occurring for weak shear. The most notable qualitative feature of the dependence arises from the introduction of a second critical wavenumber in the temporal problem as β is made larger than unity. When $\beta = 1$ the critical wavenumber appears at $k = 0$ in the temporal problem (yielding $\omega = 0$ in the spatial problem). As β is made larger the influence of the new critical point moves to higher frequencies; thus at $\beta = 1.5$ one can discern two regions of large gradient in the amplification rate. The low-frequency behaviour for integral β was treated in §4.1. In figure 7, U_0 is sufficiently small that the behaviour near $\beta = 1$ most closely resembles that in (4.2*b*) with its implication of large gradients at low frequencies; the result (4.2*a*) becomes valid only at considerably lower frequencies than can be discerned in the figure.

The above results on purely zonally directed ($l = 0$) rays suffice to illustrate most of the physically interesting aspects of the problem. In some contexts, however, it is desirable to deal with motions that have a non-trivial structure in the y-direction. In a channel geometry, for example, it would be necessary to consider motions with structure proportional to $\sin(ly)$, in which the allowable (real) values of l are determined by the channel width. The corresponding complex values of k can obviously be obtained by the same means used to solve the $l = 0$ problem. Unfortunately, there does not appear to be a Squire transformation that directly yields the amplification rates for non-zero real l in terms of those for $l = 0$.

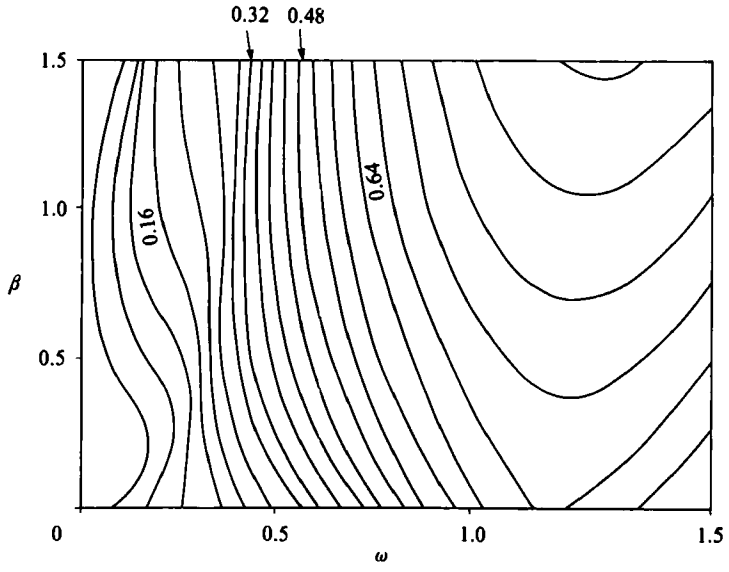

FIGURE 7. $-k_1(\omega, \beta)$ for $\omega \in [0, 1.5]$ and $\beta \in [0, 1.5]$, with $U_0 = 0.2$ and $l = 0$.

On an infinite plane, however, there is no need to decompose the response into motions that are oscillatory in y while amplifying only in the x-direction. In this case, one can more profitably deal with motions that amplify in a direction perpendicular to the lines of constant phase, specifically those with a horizontal structure of the form

$$\exp[i\mu(x\cos\theta + y\sin\theta)], \tag{5.1}$$

in which θ is a real constant and the total wavenumber μ is allowed to be complex. Then, since

$$\frac{\omega}{k} = \frac{\omega/\cos\theta}{\mu}, \tag{5.2}$$

transforming to a rotated coordinate system with $\hat{x} = x\cos\theta + y\sin\theta$ reduces the problem for μ to the previous problem for k with $l = 0$ and ω replaced by $\hat{\omega} \equiv \omega/\cos\theta$. This transformation is valid only if $\cos\theta > 0$, so that the distinction between positive and negative x used in evaluating contour integrals is not compromised. In short, the amplification rate for an oblique wave of the form (5.1) is the same as that for a zonally directed wave with a suitably defined higher frequency. This is the analogue of Squire's transformation. In the spatial problem, the result has the important implication that low-frequency oblique waves can have greater amplification rates (perpendicular to the lines of constant phase) than zonally directed waves of the same frequency, since $\hat{\omega} > \omega$ and the amplification rate increases with frequency at low frequencies.

6. Relation to structure of atmospheric variability

A detailed comparison of the stability results with atmospheric observations is outside the scope of the present work. It is nonetheless informative to consider a few quantitative predictions of the calculation, and to bring out some similarities to (and differences with) the observed structure of the atmospheric variability at low and high frequencies.

	Period (days)				
	30	15	10	5	2.5
Wavelength (km)	32000	16000	10000	4700	1600
e-folding length (km)	14000	7000	3300	1400	1000
Phase speed (m/s)	10	11	10	9	7

TABLE 1. Characteristics of amplifying disturbances arising from periodic forcing at a selection of periods

Let us first consider some salient characteristics of the spatial instabilities in dimensional terms. The lengthscale is the radius of deformation NH/f, which is of the order of 700 km in midlatitudes. The shear is more variable, and enters into the timescale N/fU_z, the velocity scale $U_z H$ and the definition of β. As noted, the results are not terribly sensitive to β. If we adopt a typical shear $U_z = (14 \text{ m/s})/(7 \text{ km})$ then the velocity scale is 14 m/s and the time scale is 0.5 days. With these values $\beta = 0.58$ and the critical frequency $\omega = 1$ corresponds to a dimensional period of about 3 days. The shear used in this estimate is typical of the zonal mean wind; thus the local values appropriate to the major Pacific and Atlantic jets are rather greater, while those appropriate to the regions between the jets are rather less. The surface wind is typically small, and is therefore subject to considerable variation. We shall present results for $U_0 = 0.2$ (dimensionally 2.8 m/s) and discuss some consequences of the sensitivity to U_0 later.

Some important properties of the amplifying disturbances corresponding to the parameter values cited above are summarized in table 1. The motions in question all exhibit eastward phase propagation with speeds of the order of 10 m/s. The e-folding length increases smoothly with increasing period, but there is still considerable amplification at the 15 day timescale. Lower frequency forcing results in larger spatial scales, to the point that the very long wavelengths encountered for the 30 day period render the consideration of local wavetrains dubious. It would also be difficult to excite the very-low-frequency motions to appreciable amplitude, as to do so would require a source that remained coherent over great distances. Thus the increase of wavelength emerges as the main factor determining the frequency below which the amplifying part of the response ceases to be of physical interest. We note that the main effect of changing the vertical shear would be to alter the time base as the non-dimensional characteristics are not too sensitive to β. For example, the results for halved shear may be obtained approximately from table 1 by doubling the periods and halving the phase speeds. This would have the effect of increasing the amplification and decreasing the wavelength of low-frequency disturbances, making them correspondingly easier to excite.

There are two studies of atmospheric variability to which these results may be compared. The first is that of Blackmon *et al.* (1984*a*, *b*), who studied the pattern of variation of the 500 mb height field subjected to various time-domain filters. It appears from this study that the properties of high-frequency (2.5–6 day) transients are generally consistent with the results shown in table 1. Specifically, the typical wavelength is about 3000 km, which falls within that predicted in the 2.5–5 day range in table 1. The typical observed phase speed is reported to be 10–15 m/s; these speeds are somewhat greater than those in table 1, but the higher speeds are generally

seen in the jet maxima, where they can be accounted for on the basis of stronger than average winds. This comparison lends further support to the already well-accepted interpretation of the high-frequency eddies as the product of baroclinic instability. A notable discrepancy though, is that comparison of results for a 2.5–4 day filter with those for a 2.5–10 day filter suggests rather less dependence of wavelength on frequency than would be expected on the basis of table 1.

The properties of low-frequency (> 10 day) eddies adduced in Blackmon *et al.* (1984*a*, *b*), on the other hand, are clearly inconsistent with the baroclinic motions described in table 1. The observed low frequency motions have wavelengths of about 7000 km, which is notably shorter than even the 10-day value given in table 1. More critically, the observed motions exhibit essentially zero phase speeds, though they show considerable downstream group propagation. As noted by Blackmon *et al.*, the low-frequency transients are more suggestive of low-frequency barotropic Rossby-wave packets. Taking the comparison further, we observe that in a *vertically sheared* atmosphere with small surface wind there exists a spectrum of low-frequency equivalent barotropic Rossby waves with $k \approx k_c$ (wavelength about 7000 km for $\beta = 0.5$), small phase speed, and rapid downstream group velocity (Held *et al.* 1985). The probable reason why the amplifying modes leave no signature in the low-frequency height pattern is that the power spectrum of the height field is very red, whence the lowest frequencies dominate the behaviour. As we have seen, the amplifying disturbances corresponding to periods much longer than 15 days have ultralong wavelengths, and are correspondingly difficult to excite.

Analysis of the height field alone does not provide any information on the vertical structure of the disturbances. Moreover, it fails to distinguish those motions predominantly responsible for the rectified eddy fluxes which affect the mean state of the atmosphere. Plumb (1986) analysed atmospheric variability in terms of a quadratic quantity measuring the influence of the transient eddies on the time-mean circulation, and obtained a picture more consonant with our results. In particular, the structure of low-frequency (> 10 day) eddies was found to be similar in all essential features to that of the high-frequency (2–10 day) eddies, which are generally accepted to represent baroclinic disturbances. Both classes of eddies are characterized by considerable baroclinic transport, the chief distinguishing feature of the low-frequency case being that the flux patterns have larger spatial scales. Diagnostic quantities of the sort employed by Plumb (1985) also, under some circumstances, provide a measure of the group velocity of the disturbances under consideration. However, this interpretation is based upon the use of the local Rossby-wave dispersion relation for unsheared flow, and may not be valid for motions satisfying more complicated dispersion relations. Thus, Plumb's finding that low-frequency motions have substantial westward group propagation relative to the mean flow in reality means only that the motions contributing to the flux are of rather large scale; this is also consistent with the characteristics of spatial baroclinic instability.

A feature of atmospheric variability common to short and medium timescales is that the maximum variance occurs in the jet exit regions, well downstream of the regions of maximum baroclinicity. In the exit regions, the surface wind and the vertical shear are relatively weak. This is suggestive of the monotonic increase of spatial amplification rate with decreasing surface wind. Because the amplification rate for $\omega = 1$ is singular in the limit of vanishing U_0, the higher-frequency motions should be particularly sensitive to U_0 (recall §4.3), and indeed, the observed high-frequency variabiity is more localized in the exit regions. Moreover, decreasing the shear with U_0 fixed increases the non-dimensional frequency and therefore

increases the amplification rate for most frequencies of interest. Thus the weak shear in the exit regions enhances the effect. Ekman friction, however, would modify this behaviour. In the presence of Ekman friction, short waves in the temporal (and hence the spatial) problem become stable when the shear is made sufficiently weak. This would put a lower limit on the values of U_0 and shear for which the mechanism discussed above can operate.

An alternate theory of the distribution of eddy activity was proposed in Pierrehumbert (1984). In that work, temporally growing free eigenmodes for a basic state varying in the streamwise direction were constructed by means of a WKB asymptotic analysis. It was shown that if the basic state, considered as a locally parallel flow, is absolutely unstable at some point (and provided certain subsidiary conditions are met) then there exist eigenmodes with the properties: (i) the growth rate is that of the absolute instability; (ii) the peak amplitude of the mode occurs downstream of the site of absolute instability; and (iii) the amplitude decays to zero exponentially at large distances upstream and downstream of the peak. When the flow is not absolutely unstable anywhere, there are no unstable eigenmodes unless periodic boundary conditions in the streamwise condition are imposed, in which case the temporal growth relies on wavepackets repeatedly passing through the zone of strong instability. The spatial formulation considered in the present work becomes attractive only when the flow is not absolutely unstable anywhere. In this formulation the variability is portrayed as a somewhat local response to stochastic forcing of a system defined on the open domain $x \in [-\infty, \infty]$. This recognizes the existence of a great deal of 'background noise' in the atmosphere, and relaxes the unrealistic assumption (necessary in the convectively unstable temporal problem) that all excitation of the instability arises from disturbances that complete a circuit of the globe. When the flow is absolutely unstable, on the other hand, it is not necessary to posit an external agent forcing the variability, as the absolute instability provides the needed excitation. The spatial theory for the convectively unstable case and the temporal theory for the absolutely unstable case share the common feature that both rely on regions of slow eddy propagation to enhance the instability. Indeed, as noted above, the regions of weak surface wind just barely miss being absolutely unstable. When applicable, the temporal eigenmode theory is more self-contained, as it yields a disturbance with a definite amplitude peak. In the forced spatial problem, on the other hand, the *amplification rate* has a sharp regional peak, but remains everywhere positive; thus an additional mechanism – perhaps Ekman friction or nonlinear saturation – must be invoked in order to reproduce the observed peak in *amplitude* near the jet exit regions.

7. Conclusions

We have shown that when a vertically sheared fluid on the quasigeostrophic β-plane is subjected to localized oscillatory forcing, a spatially amplifying train of waves is set up on the downstream side of the source. This wavetrain exhibits downstream (eastward) phase propagation and achieves its amplification by drawing energy baroclinically from the basic state; it exists in addition to the familiar (and expected) spectrum of neutral, equivalent-barotropic forced Rossby waves. At low frequencies the amplifying branch of the response is characterized by long wavelengths. The amplification rate can be physically significant even at quite low frequencies (corresponding to periods of $\approx$ 10–15 days).

In the course of solving the spatial instability problem that led to the results

described above, we have re-examined the question of absolute instability in the Charney problem. Our conclusion is that the Charney profile (with positive shear) is not absolutely unstable, provided that the wind at the ground is greater than or equal to zero. The dispersion relation $\omega(k)$ does possess a saddle point with $\mathrm{Im}(\omega) > 0$, but this does not lead to absolute instability as the two branches of $k(\omega)$ coalescing at the saddle originate on the same side of the real k-axis. Insufficient attention to this detail in the work of Farrell (1982, 1983) had lead to suggestions of absolute instability in the Charney problem with positive surface wind. The lesson to be learned from this history is applicable to *all* absolute instability calculations: methods that simply isolate selected roots of $\mathrm{d}\omega/\mathrm{d}k = 0$ without examining the topology of the images of the Bromwich contours are of little utility. Similarly, methods that do not guarantee that all relevant saddle points have been found cannot provide a reliable answer to the question of absolute instability. For all but the simplest dispersion relations, an exhaustive search of the myriad of candidate saddle points would be prohibitive. The continuation method we have described above circumvents these difficulties by identifying precisely those saddle points that come from collision of roots that originated on opposite sides of the real k-axis. This technique can be applied to any problem for which the temporal stability characteristics are known.

The lack of absolute instability for positive surface wind is important, because it implies that under typical atmospheric circumstances the forced-wave problem is physically meaningful even though the atmosphere supports baroclinic instabilities. On the spherical Earth, temporally growing instabilities will eventually dominate the forced response, but this effect will be felt only after the growing wavepackets have had time to complete a circuit of the globe. It is most likely that nonlinear effects would intervene before this time is reached.

For small to moderate positive surface winds, the spatial amplification rate has a maximum near $\omega = 1$ (dimensionally fU_z/N); at zero surface wind the amplification rate becomes infinite there, owing to the vanishing group velocity of short-wave distances. As the surface wind is made larger, the maximum growth rate moves out to approximately $\omega = U_0 k_\mathrm{m}$, where k_m is the wavenumber of maximum temporal growth rate of the Charney mode. In the spatial problem distinct Green and Charney modes do not appear. Unless the surface wind is extremely large, the spatial amplification rate has only a single maximum with respect to ω. For small or moderate surface wind, the only signature of the distinction remaining is that the rate of increase of amplification with frequency is rather small at low frequencies, but becomes larger as ω enters the Charney mode range. The approximate boundary increases roughly linearly with surface wind, and is not very sharp when the surface wind is small. Thus, in the parameter range of atmospheric interest, there is considerable continuity between the structures of response to low- and high-frequency forcing; as the frequency of the forcing is reduced, the amplification rates smoothly decrease and the wavelengths smoothly increase.

The properties of spatial baroclinic instability deduced in the present work have implications for the structure of atmospheric variability at both high and low frequencies. In the high-frequency case the primary interest lies in understanding the positions of the major storm tracks (regions of large high-frequency variance). If one thinks of the storm tracks as the ensemble averages response of the unstable system to stochastic forcing, then the spatial theory correctly predicts the intensification of amplitudes in the weak winds of the jet exit regions. We have argued that the proposed mechanism is essentially the same as the now-classic one proposed by

Landahl (1972) in explanation of localized regions of intensified variability in boundary layer flows. The spatial formulation provides a theory of storm track structure complementary to the theory based on local absolute instability proposed in Pierrehumbert (1984).

At low frequencies the characteristics of the spatial instability seem consistent with the patterns of rectified eddy fluxes seen in the analyses of atmospheric data discussed by Plumb (1986). Both the theoretical and the observational work suggest that the fluxes due to low-frequency motions are governed by processes similar to the baroclinic growth responsible for the high-frequency eddies. In addition, the low-frequency amplifying disturbances suggest a novel mechanism mediating the effect of anomalous surface conditions (particularly sea-surface temperature anomalies) on the large-scale atmospheric flow. The anomalous time-mean forcing associated with such conditions will in general be accompanied by an anomalous fluctuating component as well. The latter will excite large-scale low-frequency amplifying disturbances, which can remain coherent over great distances; in the end it may be the rectified fluxes due to such motions that force the persistent atmospheric anomaly. Indeed, there are some indications that something of this sort occurs during El Niño (Kok & Opsteegh 1985).

Detailed consideration of mechanisms for the excitation of spatial baroclinic instability will be left for future work. In particular, it will be shown that the scattering of a neutral external-mode Rossby wave from a mountain excites such an amplifying wavetrain on the downstream side of the mountain. Indeed, continued wind fluctuation of any sort over a mountain would excite the instability; this may contribute to the phenomenon of lee cyclogenesis east of the Rocky mountains. Another desirable extension would be to perform a WKB analysis of an amplifying wavetrain propagating through a medium that is slowly varying in the x- and y-directions. Such an extension would constitute a generalization of the ray-tracing theory for stationary waves developed and applied with profit by Hoskins & Karoly (1981).

Appendix A. Dispersion relation near critical point

In this appendix we determine $\omega(k)$ (and thence $k(\omega)$) for k near to one of the points k_c where $\omega = 0$. We shall carry out the computation for $U_0 = 0$ and recover the general case at the end by Galilean invariance. Our derivation closely follows that of Miles (1964*a*), except that we retain sufficient terms to yield a valid asymptotic expansion of Re (ω) for the Charney modes. The notation used is that of Pedlosky (1979), and it is assumed that the reader is familiar with the material described there. Define

$$r = \frac{1+\beta}{(1+4\mu^2)^{\frac{1}{2}}}, \tag{A 1}$$

$$n = \frac{1+\beta}{(1+4\mu_c^2)^{\frac{1}{2}}}, \tag{A 2}$$

$$a = 1-r, \tag{A 3}$$

$$\epsilon = -\pi^{-1}\tan(\pi a) = -\frac{4k_c n}{1+4\mu_c^2}(k-k_c)+\ldots$$

$$\equiv -b(k-k_c) \tag{A 4}$$

and $\mu^2 = k^2 + l^2$, where n is a positive integer. As is well known, ω vanishes when $\mu = \mu_c$. As reviewed in Pedlosky (1979), the problem can be solved in terms of confluent hypergeometric functions, and the asymptotic properties of these functions can then be used to determine the behaviour near μ_c (i.e. for small ϵ). In terms of a suitably transformed dependent variable F and independent variable ξ, the solution for small ϵ and ξ is

$$F(\xi) = \frac{1}{\xi} - n\left[\log\xi + \frac{1}{\epsilon} + R_1\right] - \frac{n(1-n)\,\xi}{2}\left[\log\xi + \frac{1-\delta_{n1}}{\epsilon} + R_2\right], \tag{A 5}$$

where δ_{n1} is the Kronecker delta and R_1 and R_2 are order-unity real constants which will not concern us. The bottom boundary condition

$$\frac{\mathrm{d}F}{\mathrm{d}\xi} - \frac{1}{2}\left[1 - \frac{n}{1+\beta}\right]F = 0 \quad \text{at } \xi = \xi_0 \tag{A 6}$$

determines the eigenvalue ξ_0, which is related to ω by

$$\xi_0 = -\frac{\omega(1+\beta)}{nk_c} + \ldots. \tag{A 7}$$

Substituting (A 5) into (A 6) yields

$$\left[\frac{n^2}{2}\frac{\beta}{1+\beta} + O(\epsilon)\right]\xi_0^2 + \frac{n^2}{2}\frac{\beta}{1+\beta}\epsilon\xi_0^2\log\xi_0 - \left[\frac{1}{2}\left(\frac{n(1+2\beta)}{1+\beta} + 1\right)\right]\epsilon\xi - \epsilon = 0, \tag{A 8}$$

in which the $O(\epsilon)$ correction to the first coefficient is purely real. The dominant balance for small ϵ is between the first and last term. A straightforward calculation yields the expansion

$$\xi_0 = A_1\epsilon^{\frac{1}{2}} + A_2\epsilon + A_3\epsilon^{\frac{3}{2}} + \ldots, \tag{A 9}$$

where

$$A_1 = -\left[\frac{2(1+\beta)}{\beta n^2}\right]^{\frac{1}{2}}, \tag{A 10}$$

$$A_2 = \frac{1+\beta}{2n^2\beta}\left[1 + \frac{n(1+2\beta)}{1+\beta}\right], \tag{A 11}$$

$$A_3 = \tfrac{1}{2}i\pi A_1 + R \tag{A 12}$$

for the unstable branch. R is a real constant, which we shall not use as the $O(\epsilon^{\frac{3}{2}})$ term in (A 9) is needed only to provide the lowest-order imaginary part of ξ_0.

Coefficients A_1 and A_3 are of course the same as determined by Miles. Miles did not compute A_2, and it seems to have been widely assumed that it is zero. Lindzen & Rosenthal (1981) pointed out that numerical evidence suggests the presence of an $O(\epsilon)$ term in the critical-point expansion, and demonstrated the existence of such a term on the basis of a WKB approximation. However, since the WKB approximation is not strictly valid for the problem at hand, it was necessary (and, as we have seen, entirely straightforward) to compute the term using asymptotic properties of the hypergeometric functions.

The relation (A 9) is easily solved for k in terms of ω. If $\Omega \equiv \omega(1+\beta)/nk_c$ then

$$k - k_c = -B_1\Omega^2 - B_2\Omega^3 + iB_3\Omega^4 + B_3'\Omega^4 + \ldots, \tag{A 13}$$

where

$$B_1 = 1/bA_1^2, \tag{A 14}$$

$$B_2 = 2A_2/bA_1^4, \tag{A 15}$$

$$B_3 = -\pi/bA_1^3, \tag{A 16}$$

and B_3' is a real constant which will not concern us. Note that these three constants are positive. Using Galilean invariance, the result for general U_0 is obtained by making the replacements

$$\Omega \Rightarrow \Omega - \frac{U_0 k_c(1+\beta)}{nk_c}, \tag{A 17}$$

$$A_2 \Rightarrow A_2 + U_0/b. \tag{A 18}$$

For positive U_0, B_2 remains positive, though B_2 can become negative if U_0 is sufficiently negative.

The above discussion presumes $k \neq 0$. In the special case when $k = 0$ is a critical point (e.g. when $l = 0$ and β is an integer), some minor modifications are required. In this case the lowest-order expressions for ϵ and ξ_0 become

$$\epsilon = -b'k^2 + \ldots, \tag{A 19}$$

$$\xi_0 = -\omega(1+\beta)/nk + \ldots, \tag{A 20}$$

where $b' \equiv 2n/(1+4\mu_c^2)$. Then, using the new forms of ϵ and ξ_0, (A 9) implies

$$\omega = -\mathrm{i}\frac{nA_1}{1+\beta}k^2 + O(k^3) \tag{A 21}$$

for $U_0 = 0$, whence

$$\omega = U_0 k - \mathrm{i}\frac{nA_1}{1+\beta}k^2 + O(k^3) \tag{A 22}$$

for the general case. To lowest order, k is then given by

$$k = \begin{cases} \dfrac{\omega}{U_0} - \mathrm{i}D\left(\dfrac{\omega}{U_0}\right)^2 & (U_0 > 0), \\ (1-\mathrm{i})\left(\dfrac{\omega}{2D}\right)^{\frac{1}{2}} & (U_0 = 0), \end{cases} \tag{A 23}$$

where $D \equiv -nA_1/(1+\beta)$. Since $D > 0$, this solution amplifies in the positive x-direction.

Appendix B. Short-wave dispersion relation

In the following we determine the behaviour of the Charney problem dispersion relation for large values of k. Our approach follows that of McIntyre (1972). The short-wave behaviour of baroclinic instability was first discussed in Miles (1964*b*), by somewhat more circuitous means.

Let $\zeta = kz$ and $\hat{\omega} = \omega - U_0 k$, so that (2.3) becomes

$$\partial_{\zeta\zeta}\phi - k^{-1}\partial_\zeta\phi + \left[k^{-1}\frac{1+\beta}{\zeta-\hat{\omega}} - 1\right]\phi = 0, \tag{B 1a}$$

$$\partial_\zeta\phi + \phi/\hat{\omega} = 0 \quad \text{at } \zeta = 0. \tag{B 1b}$$

Substituting the expansions

$$\hat{\omega} = \hat{\omega}_0 + k^{-1}\hat{\omega}_1 + \ldots, \quad \phi = \phi_0 + k^{-1}\phi_1 + \ldots \tag{B 2}$$

into (B 1) and matching like powers, the lowest-order equations are found to be

$$\partial_{\zeta\zeta}\phi_0 - \phi_0 = 0, \tag{B 3a}$$

$$\partial_\zeta\phi_0 + \phi/\hat{\omega}_0 = 0 \quad \text{at } \zeta = 0, \tag{B 3b}$$

whence

$$\phi_0 = \mathrm{e}^{-\zeta}, \quad \hat{\omega}_0 = 1. \tag{B 4}$$

At the next order the equations are

$$\partial_{\zeta\zeta}\phi_1-\phi_1 = \partial_\zeta\phi_0-\frac{(1+\beta)\phi_0}{\zeta-\hat{\omega}_0}, \tag{B 5a}$$

$$\partial_\zeta\phi_1+\phi_1 = \hat{\omega}_1 \quad \text{at } \zeta = 0. \tag{B 5b}$$

On multiplying (B 5a) by ϕ_0, integrating from $\zeta = 0$ to ∞ and making use of (B 5b) it is found that

$$\omega_1 = \tfrac{1}{2}+(1+\beta)\int_0^\infty \mathrm{d}\zeta\frac{\mathrm{e}^{-2\zeta}}{\zeta-\hat{\omega}_0} \tag{B 6}$$

As the integral in (B 6) exists only in the distributional sense, a desingularization must be specified in order to permit its evaluation. Recognizing that the neutral solution at infinite k is the limit of a weakly unstable mode, we substitute $\hat{\omega}_0+\mathrm{i}\epsilon$ for $\hat{\omega}_0$ in (B 6), where ϵ is an infinitesimal positive number. Making use of the identity

$$(\theta-\mathrm{i}\epsilon)^{-1} = \mathsf{P}(\theta^{-1})+\mathrm{i}\pi\delta(\theta), \tag{B 7}$$

where the Cauchy principal value appears in the first term and the Dirac δ-function appears in the second, (B 6) becomes

$$\hat{\omega}_1 = (\tfrac{1}{2}+(1+\beta)\,p)+\mathrm{i}\pi(1+\beta)\,\mathrm{e}^{-2}, \tag{B 8}$$

where

$$p = \mathsf{P}\int_0^\infty \mathrm{d}\zeta\frac{\mathrm{e}^{-2\zeta}}{\zeta-1} = -0.6705\ldots. \tag{B 6}$$

The imaginary part of (B 8) is identical with equation (13.14b) in Miles (1964b); Miles did not give an explicit formula for the real part. Note that the real part of $\hat{\omega}_1$ is negative for all positive β, so that the asymptotic frequency is approached from below. The extension of this derivation to an arbitrary wind profile $U(z)$ with unit shear at the ground is straightforward, and it can be shown that the formulae for the general case are identical to those presented above.

When $U_0 = 0$, solving for k in terms of ω yields

$$k = b/(\omega-1), \tag{B 7}$$

where

$$b = (\tfrac{1}{2}+(1+\beta)\,p)+\mathrm{i}\pi(1+\beta)\,\mathrm{e}^{-2}, \tag{B 8}$$

whence $k_\mathrm{r}\to+\infty$ and $k_\mathrm{i}\to-\infty$ as $\omega\to1$ from below. When $U_0 \neq 0$, k is obtained by solving a quadratic equation, which yields

$$k = \{(\omega-1)+[(\omega-1)^2-4U_0 b]^{\frac{1}{2}}\}/2U_0. \tag{B 9}$$

The choice of sign is dictated by the requirement that k become large when ω is large. Formulae (B 7) and (B 9) are valid only when the predicted k is large. For (B 7) this requires that $\omega \approx 1$. For (B 9) the requirement is that ω be order unity or greater if $U_0 \ll 1$ or that ω be large if $U_0 \geqslant O(1)$.

REFERENCES

Betchov, R. & Criminale, W. O. 1966 Spatial instability of the inviscid jet and wake. *Phys. Fluids* **9**, 359–362.

Blackmon, M. L. 1976 A climatological spectral study of the 500 mb geopotential height of the Northern Hemisphere. *J. Atmos. Sci.* **33**, 1607–1623.

Blackmon, M. L., Lee, Y.-H. & Wallace, J. M. 1984a Horizontal structure of 500 mb height fluctuations with long, intermediate and short time scales. *J. Atmos. Sci.* **41**, 961–979.

BLACKMON, M. L., LEE, Y.-H., WALLACE, J. M. & HSU, H.-H. 1984*b* Time evolution of 500 mb height fluctuations with long, intermediate and short time scales as deduced from lag-correlation statistics. *J. Atmos. Sci.* **41**, 981–991.

BRIGGS, R. J. 1964 *Electron-Stream Interaction with Plasmas*, chap. 2, 8–46. MIT Press.

CHARNEY, J. G. 1946 The dynamics of long waves in a baroclinic westerly current. *J. Meteor.* **4**, 135–162.

FARRELL, B. F. 1982 Pulse asymptotics of the Charney baroclinic instability problem. *J. Atmos. Sci.* **39**, 507–517.

FARRELL, B. F. 1983 Pulse asymptotics of three-dimensional baroclinic waves. *J. Atmos. Sci.* **40**, 2202–2209.

GASTER, M. 1962 A note on the relation between temporally increasing and spatially increasing disturbances in hydrodynamic stability. *J. Fluid Mech.* **14**, 222–224.

GASTER, M. 1965 On the generation of spatially growing waves in a boundary layer. *J. Fluid Mech.* **22**, 433–441.

HELD, I. M., PANETTA, R. L. & PIERREHUMBERT, R. T. 1985 Stationary external Rossby waves in vertical shear. *J. Atmos. Sci.* **42**, 863–883.

HELD, I. M., PIERREHUMBERT, R. T. & PANETTA, R. L. 1986 Dissipative destabilization of external Rossby waves. *J. Atmos. Sci.* **43**, 388–396.

HOGG, N. G. 1976 On spatially growing baroclinic waves in the ocean. *J. Fluid Mech.* **78**, 217–235.

HOSKINS, B. J. & KAROLY, D. J. 1981 The steady linear response of a spherical atmosphere to thermal and orographic forcing. *J. Atmos. Sci.* **38**, 1117–1318.

HUERRE, P. & MONKEWITZ, P. A. 1985 Absolute and convective instabilities in free shear layers. *J. Fluid Mech.* **159**, 151–168.

KOK, C. J. & OPSTEEGH, J. P. 1985 Possible causes of anomalies in seasonal mean circulation patterns during the 1982–83 El Niño Event. *J. Atmos. Sci.* **42**, 677–694.

LANDAHL, M. T. 1972 Wave mechanics of breakdown. *J. Fluid Mech.* **56**, 773–802.

LINDZEN, R. S. & ROSENTHAL, A. J. 1981 A WKB asymptotic analysis of baroclinic instability. *J. Atmos. Sci.* **38**, 619–629.

MCINTYRE, M. 1972 Baroclinic instability of an idealized model of the polar night jet. *Q. J. R. Met. Soc.* **98**, 165–173.

MERKINE, L.-O. 1977 Convective and absolute instability of baroclinic eddies. *Geophys. Astrophys. Fluid Dyn.* **9**, 129–157.

MERKINE, L.-O. 1982 The stability of quasi-geostrophic fields induced by potential vorticity sources. *J. Fluid Mech.* **116**, 315–342.

MICHALKE, A. 1965 On spatially growing disturbances in an inviscid shear layer. *J. Fluid Mech.* **23**, 521–544.

MILES, J. 1964*a* A note on Charney's model of zonal-wind instability. *J. Atmos. Sci.* **21**, 451–452.

MILES, J. 1964*b* Baroclinic instability of the zonal wind. *Rev. Geophys.* **2**, 155–176.

PEDLOSKY, J. 1979 *Geophysical Fluid Dynamics*. Springer.

PIERREHUMBERT, R. T. 1984 Local and global baroclinic instability of zonally varying flow. *J. Atmos. Sci.* **41**, 2141–2162.

PLUMB, R. A. 1986 Three-dimensional propagation of transient quasigeostrophic eddies and its relationship with the eddy forcing of the time-mean flow. *J. Atmos. Sci.* (in press).

SARDESHMUKH, P. D. & HOSKINS, B. J. 1985 Vorticity balances in the tropics during the 1982–83 El Niño–Southern Oscillation event. *Q. J. R. Met. Soc.* **111**, 261–278.

THACKER, W. C. 1976 Spatial growth of Gulf Stream meanders. *Geophys. Astrophys. Fluid Dyn.* **7**, 271–295.